Applied Catalysis B: Environmental 134–135 (2013) 185–192

Contents lists available at SciVerse ScienceDirect

Applied Catalysis B: Environmental

journal homepage: www.elsevier.com/locate/apcatb

Photoelectrocatalytic properties of Cu^{2+}-doped TiO_2 film under visible light

Meihong Zhang, Shuai Yuan*, Zhuyi Wang, Yin Zhao, Liyi Shi*

Research Center of Nanoscience and Nanotechnology, Shanghai University, 99 Shangda Road, Shanghai 200444, PR China

ARTICLE INFO

Article history:
Received 26 September 2012
Received in revised form 8 January 2013
Accepted 14 January 2013
Available online 23 January 2013

Keywords:
Photoelectrocatalysis
Cu^{2+} ion doping
TiO_2 film
Visible light

ABSTRACT

Cu^{2+}-doped TiO_2 film on stainless steel substrates was prepared using sol–gel method. Based on XRD and SEM analysis results, the as-prepared film was mainly in anatase phase. The film was smooth and the thickness of the film was about 2 μm. The UV–vis absorption of Cu^{2+}-doped TiO_2 was extended to visible range, which is favorable for the utilization of solar light. The photoelectrochemical properties of the samples were investigated via electrochemical impedance spectrum (EIS). The EIS plots demonstrated that the Cu^{2+}-doped TiO_2 can be excited under visible light irradiation and the photo-generated electron–hole pairs can be separated efficiently by applying an external bias. The degradation experiments for methylene blue and methyl orange in different processes showed that the photo-response range of TiO_2 could be extended by doping Cu^{2+} ion and the photocatalytic activity of TiO_2 could be enhanced with the help of a forward bias.

1. Introduction

TiO_2 is the most widely used photocatalyst due to its low cost, chemical stability, and excellent catalytic properties [1–4]. Nevertheless, the use of TiO_2 powders dispersed into aqueous media as a catalyst presents relevant technological drawbacks such as the difficulty of catalyst recovery, the low utilization efficiency of visible light (only absorb UV light), and the high recombination rate of photo-generated electron–hole pairs [5]. These drawbacks are crucial indeed for viable applications in water treatments on a large scale.

To overcome the problem of catalyst recovery and recycle, TiO_2 film, a type of immobilized photocatalyst, is attracting great attention in the area of photocatalysis [6–13].

TiO_2 can absorb only UV light ($\lambda < 387$ nm), and UV light is just a small part of the whole solar energy. The absorption of TiO_2 can be extended to visible range by coupling with other semiconductors or doping non-metal or metal ions (such as B, C, and N, Fe^{3+} and Zn^{2+} [14–20]). Especially, the activity of Cu^{2+} ion as a catalyst in many oxidation and reduction reactions makes it very attractive as a doping agent for titania [21]. Based on our previous research, the Cu^{2+} ion doping can expand the absorption band edge to visible range and enhance the photocatalytic activity of TiO_2 under the visible light irradiation. So, it is promising to prepare the visible light sensitized TiO_2 photocatalyts by taking advantage of both film-form with easy recyclability and Cu^{2+} doping with enhancing visible light absorption.

The random diffusion of photo-generated electrons and holes in the TiO_2 nanocrystals results in the high recombination rate and low photocatalytic efficiency. The separation of electron–hole pairs can be promoted via photoelectrocatalysis (PEC) technique by electron transfer under the control of an external circuit in PEC process, which is possible when the photocatalyst is deposited on the electrically conducting substrates [22]. However, most researchers focus on the PEC properties of TiO_2 under UV light irradiation and few papers have reported the PEC properties of TiO_2 film under visible light irradiation so far. If external bias was applied on the visible light sensitized TiO_2 film on conducting substrates, the photocatalytic activity should be improved remarkably due to the inhibited electron–hole pair recombination process.

In this paper, the Cu^{2+}-doped TiO_2 film on the stainless steel was prepared via a sol–gel method, followed by the investigation of the photocatalytic (PC), electrochemical (EC) and photoelectrocatalytic (PEC) properties under UV or visible light irradiation, using methylene blue (MB) and methyl orange (MO) as the model organic pollutants in water. Furthermore, the effects of Cu^{2+} doping and applied external bias on the generation of electrons and holes and separation were discussed by the electrochemical analysis to obtain insights on improving the PEC performance of TiO_2 film for the purification of organic pollutants in waste water under visible light irradiation.

2. Experimental

2.1. Materials

Tetrabutyl titanate ($Ti(OBu)_4$), polyethylene glycol with molecular weight 400 (PEG 400), diethanolamine (DEA), cupric nitrate

* Corresponding authors. Tel.: +86 21 66134852; fax: +86 21 66134852.
E-mail address: s.yuan@shu.edu.cn (S. Yuan).

0926-3373/$ – see front matter © 2013 Elsevier B.V. All rights reserved.
http://dx.doi.org/10.1016/j.apcatb.2013.01.024

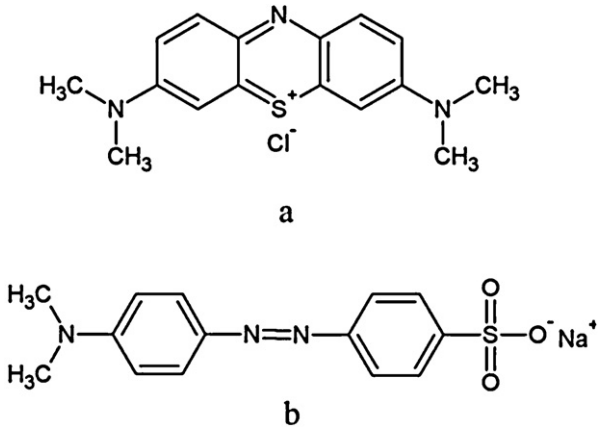

Scheme 1. Molecular structure of methylene blue (a) and methyl orange (b).

trihydrate ($Cu(NO_3)_2{\cdot}3H_2O$), vinyltriethoxysilane (A151), ethanol, methylene blue (MB) and methyl orange (MO) were purchased from Sinopharm Chemical Reagent Co. Ltd. (China) without further purification. Stainless steel was purchased from Anping Hua Yu Wire Mesh Factory (China).

2.2. Preparation of Cu^{2+}-doped TiO_2 film electrodes

The Cu^{2+}-doped TiO_2 film electrode was prepared by sol–gel method, using dip-coating as the coating way.

First, $Ti(OBu)_4$ was added to the mixture of ethanol, DEA and PEG 400 under vigorous stirring to form a solution. Then a certain amount of $Cu(NO_3)_2{\cdot}3H_2O$ was added to the solution, followed by adding A151. The volume ratio of $Ti(OBu)_4$, DEA, PEG 400, A151 and ethanol was 2.5:2:1.8:0.4:10. The molar ratio of Cu and Ti was 0.05:100.

Before deposition, the stainless steel substrates (2 cm × 9 cm) were sequentially cleaned in an ultrasonic bath with acetone and ethanol, followed by rinsing in distilled water and drying in an oven.

The films were dip-coated on stainless steel substrates, with independently adjustable dipping (10 cm/min) and withdrawn (60 cm/min) rates. Each sample was dipped into the as-prepared sol twice. After each dipping process, samples were dried at 140 °C for 15 min. Then the samples were placed into furnace for calcination. The furnace temperature increased at a ramp rate of 5 °C/min to 450 °C and held at this value for 2 h. Finally the samples were cooled down naturally in the furnace to room temperature.

Pure TiO_2 film electrode as a reference was prepared in the same way, except that no $Cu(NO_3)_2{\cdot}3H_2O$ was added to the above solution.

2.3. Degradation experiments

In order to investigate the PEC properties of the pure TiO_2 and Cu^{2+}-doped film, two kinds of dyes were chosen as model dyeing pollutants in our experiments including methylene blue (MB) and methyl orange (MO). The former is a cationic dye and the latter is an anionic dye. Scheme 1 shows the molecular structures of MB and MO. The degradation experiments were performed by using 50 ml MB or MO solutions with both of initial dye concentrations of 6 mg/L. The experiments were carried out in a quartz tube (3 cm (φ) × 12 cm (L)) equipped with the pure TiO_2 or Cu^{2+}-doped TiO_2 film as photoanode and Ti foil at a distance of 1 cm as cathode. The irradiation sources were two UV lamps (λ_{max} = 365 nm, 8 W, Royal Dutch Philips Electronics Ltd) or two fluorescent lamps (λ = 400–800 nm, 14 W, Royal Dutch Philips Electronics Ltd), with a light intensity of 10.0 mW/cm^2 (measured by a radiometer, LP-3 A, Beijing Wuke Photoelectric Technique Co., Ltd) by adjusting the distance between the lamp and reactor.

Prior to the degradation reaction, the solution was magnetically stirred in dark for 1 h to establish an adsorption–desorption equilibrium, so the loss of the compound due to adsorption can be taken into account. Then the solution was illuminated and applied + 1.0 V external potential (controlled using a power supply) on the electrode. The dye concentration of the solution was measured every 30 min. The degradation rate on dyes was calculated as follows:

$$D = \frac{A_0 - A}{A_0} \times 100\% \quad (1)$$

where A_0 and A are the initial and final absorbance at 664 nm for MB and 463 nm for MO, respectively.

All degradation experiments were performed under ambient atmosphere and vigorous stirring. As the reference, the PC experiment was performed by using the system without applying an external bias, and the EC experiment was performed without light irradiation.

2.4. Characterization of the pureTiO_2 and Cu^{2+}-doped TiO_2 film electrodes

The pure TiO_2 and Cu^{2+}-doped TiO_2 powder were scraped off from the stainless steel substrates. The crystallinity was detected by D/Max-2550 X-ray diffraction meter (Rigaku Corporation, Japan) and Laser Micro-Raman spectrometer (InVia plus, Renishaw plc, UK) with the laser wavelength of 514.5 nm. The surface and cross-section of the films was examined using scanning electron microscope (SEM) with energy-dispersive X-ray analysis (EDX) (JSM-6700F field emission scanning electron microscopy, JEOL, Japan). X-ray photoelectron spectroscopy (XPS) measurements were carried out under ultra-high vacuum (<10^{-6} Pa) at a pass energy of 93.90 eV on a Perkin-Elmer PHI 5000 C ESCA system equipped with a dual X-ray source by using Mg–Ka (1253.6 eV) anode. All binding energies are calibrated by using contaminant carbon (C 1s = 284.6 eV) as a reference. Optical properties of the samples were determined by measuring the UV–vis absorbance spectra using a UV-2501 PC spectrometer (Shimadzu, Japan) Spectrumlab.

The electrochemical studies were performed using a standard three-electrode cell containing 0.1 M sodium sulfate (Na_2SO_4) solution, and measured by an electrochemical workstation (SI 1287, Solartron analytical, UK). The potentials were measured relative to a standard calomel reference electrode (SCE). Electrochemical impedance spectroscopy (EIS) curves of samples at the open-circuit potential and under external bias (+20 mV) were obtained in the dark, under UV (λ_{max} = 365 nm) or visible (λ = 400–800 nm) light irradiation with a light intensity of 10.0 mW/cm^2. The EIS data were evaluated and fitted to the suggested equivalent circuit. The frequency range was from 0.01 Hz to 100 MHz and the irradiated area of the working electrode is 1 cm^2.

3. Result and discussion

3.1. Structure of the pure TiO_2 and Cu^{2+}-doped TiO_2 film electrodes

The XRD patterns (Fig. 1a) for the particles collected by scraping off the pure TiO_2 and Cu^{2+}-doped TiO_2 from the electrodes confirm that both of the samples are well crystallized. According to JCPDS data, the peaks at 25.4° (1 0 1), 38.5° (1 1 2), and 48.6° (2 0 0) are the characteristic reflections for anatase. The grain size of the samples calculated by Scherrer's formula is about 60 nm. No peak for CuO is found due to the low doping amount.

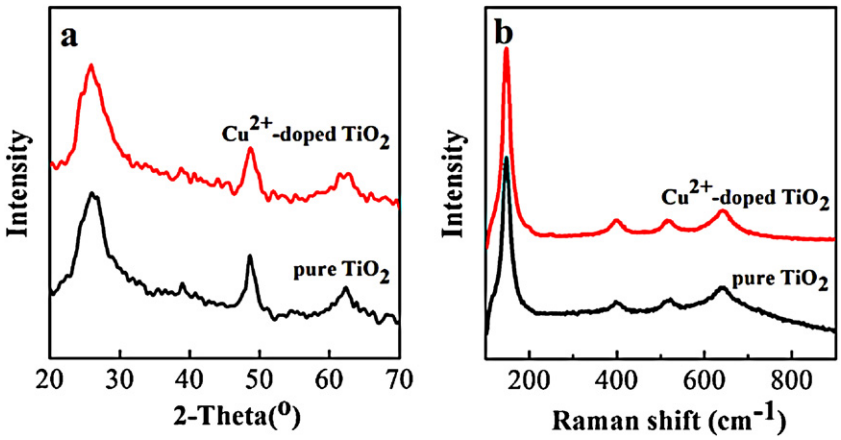

Fig. 1. XRD patterns of the particles (a) and Raman scattering spectra of the films (b) for the pure TiO_2 and Cu^{2+}-doped TiO_2.

The Raman scattering spectra of the pure TiO_2 and Cu^{2+}-doped TiO_2 films are shown in Fig. 1b. It shows the characteristic peaks assigned to anatase structure with strong Raman active optical phonon vibrations, which is consistent with the XRD analysis. The peaks at 145.8, 396.3, 517.2 and 639.8 cm^{-1} are ascribed to the Raman active vibration of E_g ($\upsilon 6$), B_{1g} ($\upsilon 4$), $A_{1g} + B_{1g}$ ($\upsilon 2 + \upsilon 3$) and E_g ($\upsilon 1$), respectively.

Fig. 2 shows SEM images of the deposited pure TiO_2 and Cu^{2+}-doped TiO_2 films on stainless steel substrates (Fig. 2c and d) and their cross-section (Fig. 2a and b). These images illustrate a general view of morphology of the pure TiO_2 and Cu^{2+}-doped TiO_2 particles on the substrates as well as film thickness. The film coverage is quite uniform and the thickness of the films is about 2 μm. The uniform coverage can guarantee a high surface area as well as electron transport through the films, important parameters for the photoelectrocatalytic efficiency of a film electrode.

The XPS analysis was carried out to determine the surface composition of the pure TiO_2 and Cu^{2+}-doped TiO_2 samples to identify the valence states of various species present therein. X-ray photoelectron spectra of the samples are shown in Fig. 3. The peak intensity of Cu $2p_{3/2}$ transition cannot be found in the XPS spectrum of Cu^{2+}-doped TiO_2 sample. Although the doping amount of Cu^{2+} is too low to be detected, the effects of doping process could be reflected by XPS results. As can be seen in Fig. 3a, for the pure TiO_2, the binding energies of Ti $2p_{3/2}$ and Ti $2p_{1/2}$ are at approximately 458.4 eV and 464.2 eV, respectively, which is assigned to the presence of typical Ti^{4+} [23]. For the Cu^{2+}-doped TiO_2, Ti $2p_{3/2}$ transition shifts to lower binding energies, which is due to the electronic interaction between Cu and Ti in nanocomposites [24]. These results means Cu^{2+} ions are well dispersed in the TiO_2 lattice instead of being assemble at the surface of TiO_2 [25].

Also, the doping process leads to the changes in the O species. The XPS spectra of O 1s for the samples (Fig. 3b) are also fitted

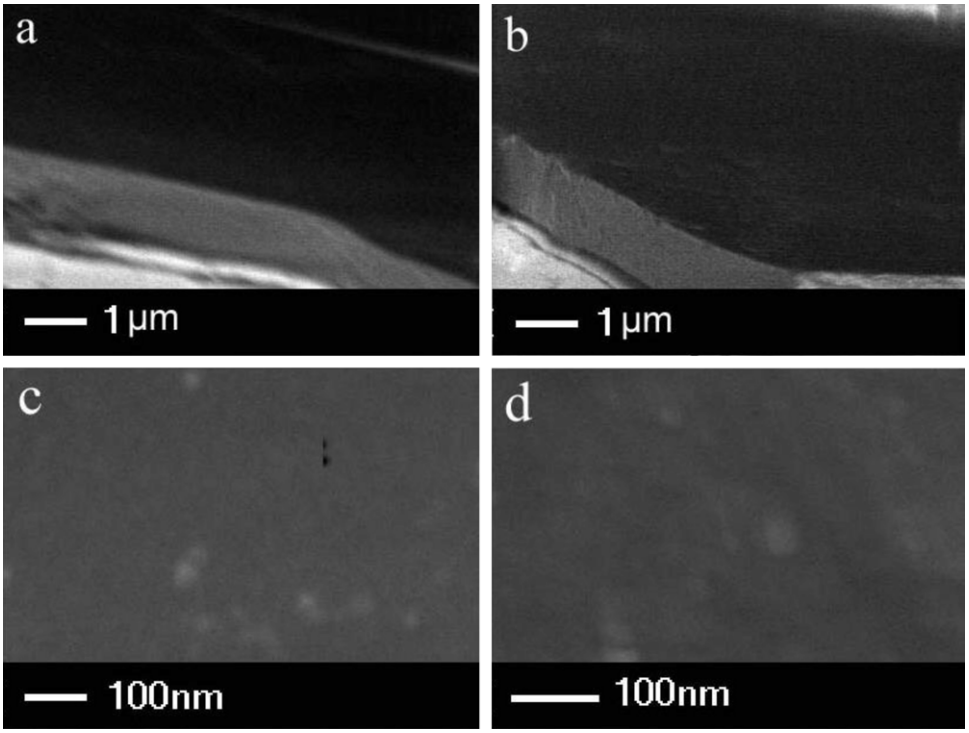

Fig. 2. SEM images of the deposited pure TiO_2 and Cu^{2+}-doped TiO_2 films on stainless steel substrates: (a) cross-section of the pure TiO2 films, (b) cross-section of the Cu^{2+}-doped TiO_2 films, (c) top-view of pure TiO_2 films on stainless steel substrates, (d) top-view of Cu^{2+}-doped TiO_2 films on stainless steel substrates.

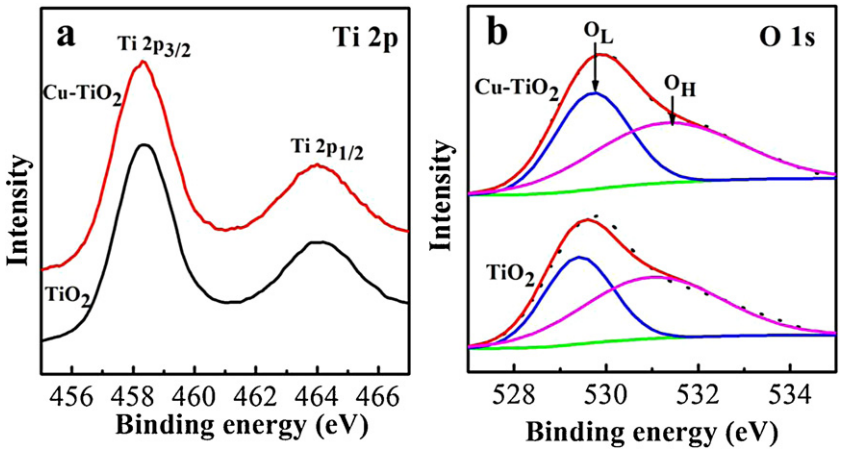

Fig. 3. X-ray photoelectron spectra of the samples: (a) Ti region; (b) O region.

Table 1
Surface analysis by XPS spectra for the pure TiO_2 and Cu^{2+}-doped TiO_2.

Samples	Binding energe (eV)			O_L (%)	O_H (%)
	Ti $2p_{3/2}$	O_L 1s(Ti-O)	O_H 1s(O-H)		
The pure TiO_2	458.4	529.4	531.0	49.2	50.8
Cu^{2+}-doped TiO_2	458.3	529.8	531.4	44.1	55.9

well by two asymmetric Gaussian curves which are denoted as lattice oxygen (O_L) and surface hydroxyl oxygen (O_{OH}), respectively [26]. Table 1 shows the XPS data of Ti and O elements at the surface of the pure TiO_2 and Cu^{2+}-doped TiO_2 samples. The content of O_{OH} is developed when Cu^{2+} is doped into TiO_2, which can be attributed to the increase of oxygen vacancies induced by doping process. Besenbacher's group found oxygen vacancies in the surface layer are shown to dissociate adsorbed H_2O through the transfer of one proton to a nearby oxygen atom, forming two hydroxyl groups for every vacancy [27]. So the content of O_{OH} will increase with more oxygen vacancies induced by Cu^{2+}.

The UV–vis absorption spectra for the particles collected by scraping off the pure TiO_2 and Cu^{2+}-doped TiO_2 film from the electrodes are shown in Fig. 4. The absorption spectra of Cu^{2+}-doped TiO_2 exhibit a red shift to visible range. The enhanced ability to absorb visible light makes TiO_2 a promising photocatalyst for visible light driven applications.

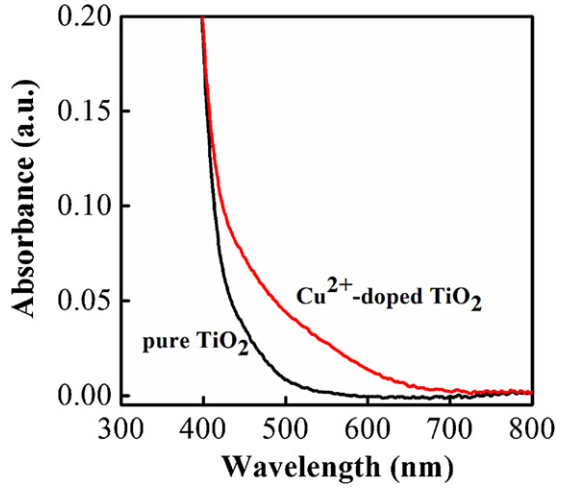

Fig. 4. UV–vis absorption for the particles for the pure TiO_2 and Cu^{2+}-doped TiO_2 films.

In addition to the utilization of light, the photo-generated charges transfer and recombination properties are also critical to photocatalytic and photoelectrocatalytic processes [1]. The photoelectrochemical properties of the samples were investigated to reveal the charge transfer and recombination processes. The electrochemical impedance spectrum (EIS) is demonstrated as a powerful method for studying the charge transfer and recombination processes at semiconductor/electrolyte interfaces in the photocatalytic and photoelectrocatalytic processes on TiO_2 electrodes [28].

The EIS responses of the pure TiO_2 and Cu^{2+}-doped TiO_2 film electrodes are presented as Nyquist plots corresponding to the imaginary part Z'' versus the real part Z' of the complex impedance Z (as shown in Fig. 5). EIS plot with and without light irradiation for each sample was measured at open-circuit potential and under external bias (+20 mV), respectively.

It can be seen that the Nyquist plots of samples are composed of a circular arc and the diameter of the loops is largely reduced when Cu^{2+} is doped into TiO_2. This phenomenon also appears when the samples are under light irradiation, especially under UV light irradiation. Under light irradiation, the photo-generated electrons and holes will be produced from the excited pure TiO_2 or Cu^{2+}-doped TiO_2 film electrodes. The photo-generated electrons will flow into outside circuit. Thus, the interface resistance will be reduced and the diameter of loops reduces. On the other hand, the diameter of loops reflects the transferring rate of electron thus reflects the photocatalytic reaction rate.

Fig. 5d–f shows the EIS responses of pure TiO_2 and Cu^{2+}-doped TiO_2 film electrodes measured under external bias (+20 mV). With the help of external bias, the photo-generated electron–hole pairs are separated efficiently, and thus the semicircle sizes of both film electrodes decrease sharply in the EIS plane. From another aspect, applied external bias will also increase the band bending of both samples and change the width of space charge layer which is also critical to the separation of photo-generated electron–hole pairs [29]. The electron–hole pairs within the space charge layer are efficiently separated by the electric field, which is favorable to the high photocatalytic efficiency.

The equivalent circuit for samples is depicted in the inset of Fig. 5a. In the equivalent circuit, R_b denotes the bulk resistance of the electrolyte and electrodes, corresponding to the resistance value of the high frequency intercept of the semicircle with the real axis; R_i is the resistance formed at the interfaces of the electrodes which include two parts. One of them formed at the highly charged states due to the passivation reaction between the electrolyte and the surface of the electrode, and the other is dependent

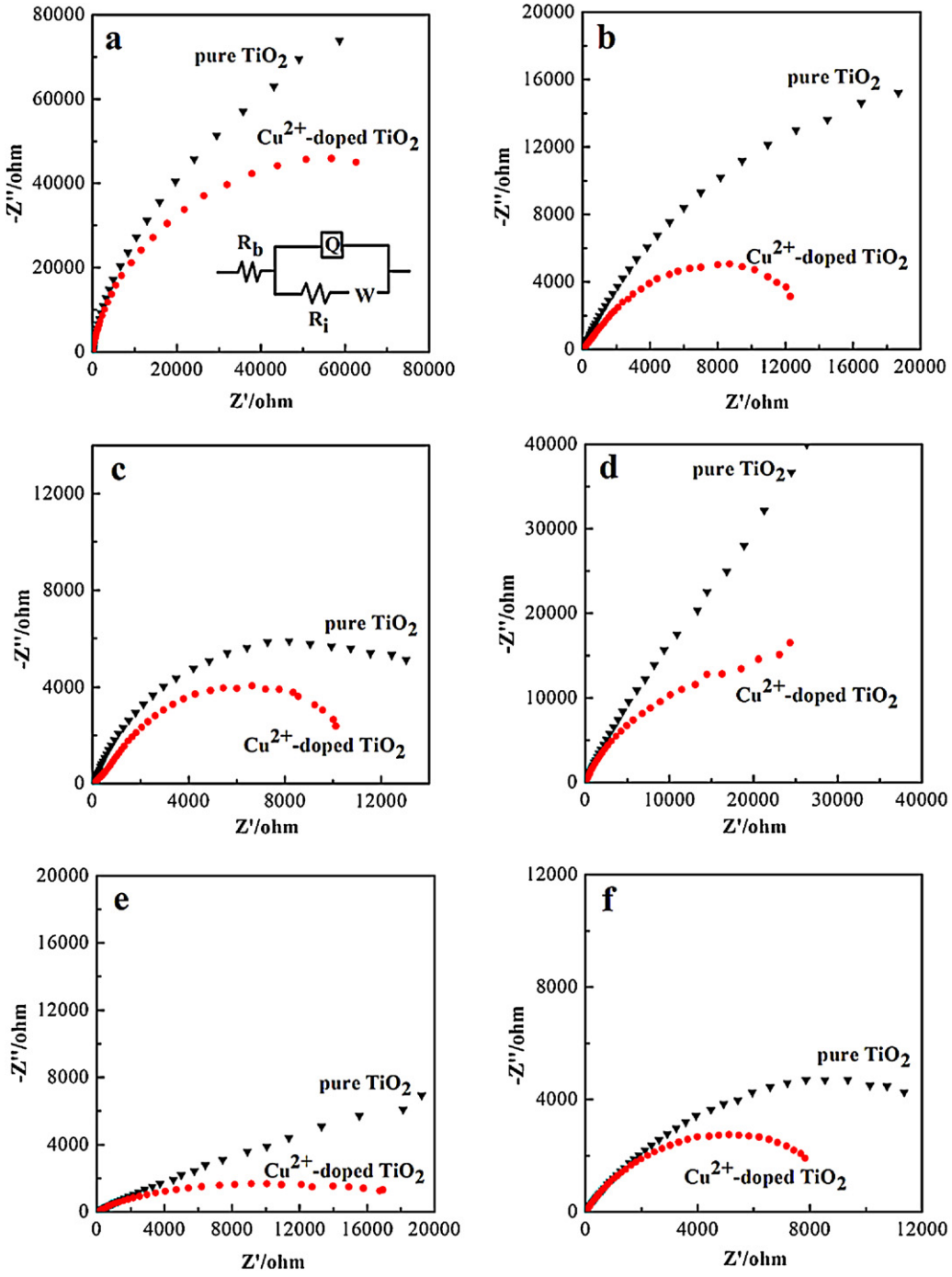

Fig. 5. The EIS responses (Nyquist plots) of the pure TiO_2 and Cu^{2+}-doped TiO_2 film electrodes with and without light irradiation, measured at open-circuit potential and under external bias (+20 mV), respectively:(a) at open-circuit potential in the dark, (b) at open-circuit potential under visible light irradiation, (c) at open-circuit potential under UV light irradiation, (d) at applied external bias in the dark, (e) at applied external bias under visible light irradiation, (f) at applied external bias under UV light irradiation.

on the double layer capacitance and the charge transfer resistance [30].

Fitted parameters of the pure TiO_2 and Cu^{2+}-doped TiO_2 film samples at open-circuit potential and under external bias (+20 mV) according to the equivalent circuit depicted in the inset of Fig. 5a are shown in Table 2. Under the given measure conditions, the bulk resistance R_b changes from 25.74 Ω/cm^2 to 60.58 Ω/cm^2, which can be ignored compared with R_i, and the R_i values are decreased significantly after applying UV or visible light irradiation and external bias. It is noticeable that R_i is decreased sharply to 0.871×10^4 Ω/cm^2 when UV light irradiation and external bias are applied, which imply a stronger driving force to increase the charge separation rate than the samples without applied light irradiation and external bias.

When the interface of semiconductor/solution is effectively illuminated, the electron–hole pairs separate under the effect of the space charge field, that is, the electrons are pulled into the internal semiconductor, and the holes are pushed to the surface of the electrode. At the open-circuit potential, the generation and separation of electron–hole pairs will result in the space charge electric field weakened, and thus with the decrease in the degree of energy band bending (compared to the dark state). The energy

Table 2
Fitted parameters of the pure TiO_2 and Cu^{2+}-doped TiO_2 film samples at open-circuit potential and under external bias (+20 mV) according to the equivalent circuit in the inset of Fig.4a.

Sample	External bias (mV)	Irradiation condition	R_b (Ω/cm^2)	R_i ($\times10^4\ \Omega/cm^2$)
Pure TiO_2 film electrode	0	Dark	27.61	10.16
	0	Visible light	60.58	2.184
	0	UV light	51.03	1.798
	20	Dark	45.19	2.578
	20	Visible light	43.39	2.106
	20	UV light	31.8	1.256
Cu^{2+}-doped TiO_2 film electrode	0	Dark	32.49	7.936
	0	Visible light	46.46	2.171
	0	UV light	25.74	1.596
	20	Dark	43.62	3.989
	20	Visible light	51.69	1.487
	20	UV light	33.51	0.871

band bending reaches a new steady state in the continuous light condition. The energy band bending in the space–charge layer is just the driving force of semiconductor photocatalysis. The photo-generated charge carriers in the space–charge layer drift under the effect of electric field. The non-equilibrium electrons move toward the body to flow to the counter electrode through an external circuit, and the non-equilibrium holes move toward the surface and react with the active particles in the solution to generate photocurrent. In order to make the photo-generated charge carriers quickly separated, a certain potential is applied to the semiconductor/solution to form overpotential on the electrode. The overpotential changes the potential drop of the semiconductor space charge region, thus changing the width of space–charge layer of the semiconductor [30]. This reduces the recombination of photo-generated electron–hole pairs, so that the concentration of photo-generated charge carrier on the semiconductor surface is increased (sometimes this is increased up to several orders of magnitude). Therefore, the effective photocatalytic reaction can be performed on the semiconductor/solution interface, which is also the principle of electrically assisted photocatalysis.

3.2. Photoelectrocatalytic and photocatalytic activities of the pure TiO_2 and Cu^{2+}-doped TiO_2 film electrodes

The results of different processes including electrochemical (EC), photocatalytic (PC) and photoelectrocatalytic (PEC) degradation performances on different dyes for the pure TiO_2 and Cu^{2+}-doped TiO_2 film electrodes are summarized in Table 3 and Fig. 6.

Fig. 6 shows that the degradation of MB and MO in various processes under the given conditions corresponds to a pseudo-first-order reaction. Pseudo-first-order kinetics was assumed to calculate the corresponding degradation rate constant (k)

$$\ln\frac{C}{C_o} = -kt \quad (2)$$

where C_o is the original MB or MO concentration after the adsorption–desorption reached equilibrium (mg/L), C is the concentration (mg/L) at a given time t (min) and k is the first-order degradation rate constant (min^{-1}). Half-life, $t_{1/2}$ (min), can be calculated from k by using the following equation

$$t_{1/2} = \frac{\ln 2}{k} \quad (3)$$

the ranking of rate constant k of various processes for both MB and MO was UPEC > VPEC > UPC > VPC > EC process.

Compared with the pure TiO_2 film electrode, the Cu^{2+}-doped TiO_2 film electrode shows better PC and PEC activities. The gap is pronounced in the PEC process under visible light irradiation. Yu [21] reported that the photo-response wavelength of Cu^{2+}-doped TiO_2 expanded to visible region. In general, a doping level is formed after Cu^{2+} is doped into TiO_2, which reduce the band gap energy. Thus the electrons in valence band can be excited by visible light and the photocatalytic activity under visible light can be improved [31], which is verified by the UV–vis absorption of the pure TiO_2 and Cu^{2+}-doped TiO_2 particles (Fig. 4). The visible light-induced activity of the Cu-doped TiO_2 resulted from the electron excitation and charge separation is due to the transition from the TiO_2 valence band to the Cu^{2+} impurity states [32].

In the case of different processes, the degradation rate constant of EC and PC processes were clearly much smaller than that of PEC process. In PEC process, with the applied external bias, photo-generated electrons are driven via an external circuit and the rapid recombination of electrons and holes was prevented [33]. Consequently, photocalalytic activity is able to be improved. The

Table 3
The result of different processes degradation performances on different dyes for the pure TiO_2 and Cu^{2+}-doped TiO_2 film electrodes.

Photocatalyst	Reaction condition	k ($\times10^{-4}\ min^{-1}$)		$t_{1/2}$ ($\times10^2$ min)	
		MB	MO	MB	MO
Pure TiO_2 film electrode	EC	2.51	2.92	27.6	23.70
	VPC	2.59	3.17	26.8	21.90
	UPC	8.96	9.14	7.74	7.58
	VPEC	10.70	9.57	6.48	7.24
	UPEC	25.30	25.80	2.74	2.69
Cu^{2+}-doped TiO_2 film electrode	EC	1.78	2.20	38.9	31.5
	VPC	2.61	4.03	26.6	17.2
	UPC	8.93	10.5	7.76	6.60
	VPEC	19.10	24.8	3.63	2.79
	UPEC	25.40	31.4	2.73	2.21

EC, VPC, UPC, VPEC, UPEC correspond to electrochemical process, photocatalysis under visible light irradiation, photocatalysis under UV light irradiation, photoelectrocatalysis under visible light irradiation, and photoelectrocatalysis under UV light irradiation, respectively.

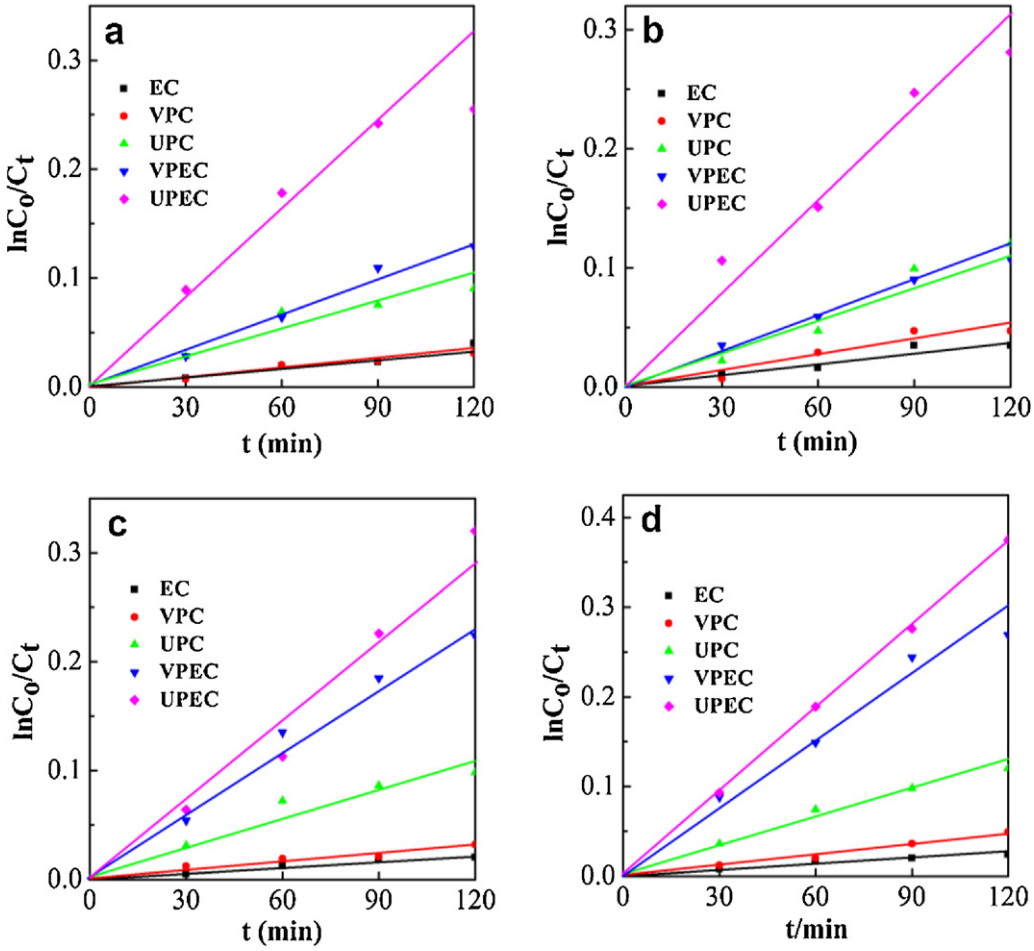

Fig. 6. First-order kinetics for the MB and MO degradation on the samples: (a) MB on the pure TiO_2 film, (b) MO on the pure TiO_2 film, (c) MB on the Cu^{2+}-doped TiO_2 film, and (d) MO on the Cu^{2+}-doped TiO_2 film.

application of an anodic bias to TiO_2 film photoelectrode under the given conditions can provide a driving force to the separation of photo-generated electron–hole pairs efficiently and can also increase the adsorption of anionic dye on photo-anode [34]. By applying an external anodic potential (+1.0 V) to the photoelectrode under UV light irradiation, the degradation rate constant increased from 8.93×10^{-4} min^{-1} to 2.54×10^{-3} min^{-1} for MB, and from 1.05×10^{-3} min^{-1} to 3.14×10^{-3} min^{-1} for MO, respectively.

3.3. Mechanism of PEC process

The pathway for PEC process can be divided into three steps: adsorption of TiO_2 film electrodes, photocatalytic reaction, and electron transfer.

First, the adsorption property is a significant factor for photoelectrocatalyst. In general, the positively charged TiO_2 film electrode favors the adsorption of negatively charged particles, due to the electrostatic attraction.

Then, when TiO_2 film electrodes are irradiated with excitation light source, some electrons are excited from the valence band (VB) to the conductive band (CB), leaving highly oxidative holes in the VB and negative sites in the CB [35].

The adsorbed organic compounds can be oxidized directly by the holes or hydroxyl radicals on the electrode surface, while the excited electrons and holes may recombine [36]. The reactions are as follows [37] (Scheme 2a):

$$e_{CB}^{-} + h_{VB}^{+} \rightarrow TiO_2 + \text{heat} \quad (4)$$

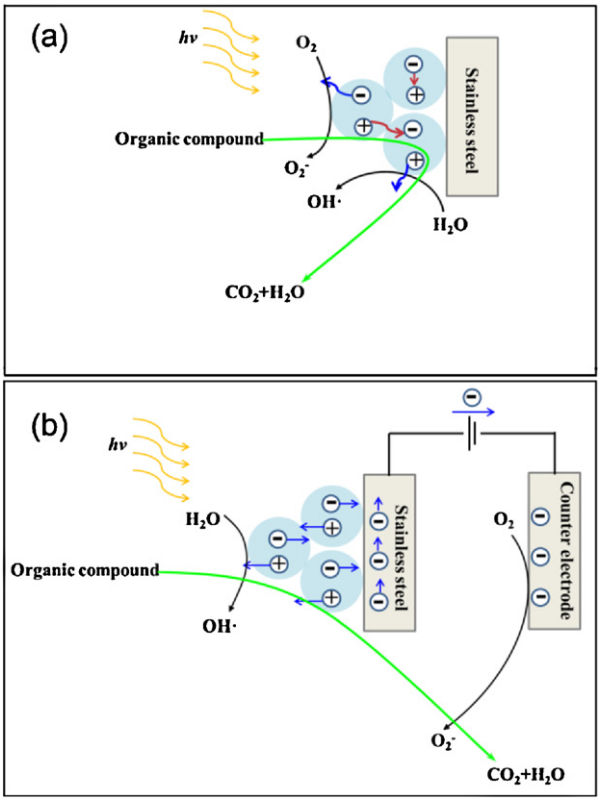

Scheme 2. Illustration of photocatalytic (a) and photoelectrocatalytic (b) processes.

When an external bias is applied to the TiO_2 film electrodes, the moving direction of photo-generated electrons and holes changed from random to orientation (as shown in Scheme 2b). Therefore, the collision and recombination opportunities of photo-generated electrons and holes reduced greatly, which is responsible to the higher PEC activity of photoelectrodes.

The electron transfer for the PEC oxidation process involves two major pathways. The first is the electron transfer in TiO_2 film itself, and the second is the electron injection at the interface (photohole capture) [38]. Applying a proper external bias favors to enhance both of the electron transfer pathways, thus favors to improve the photocatalytic efficiency.

4. Conclusion

Cu^{2+}-doped TiO_2 film electrode on stainless steel substrates was prepared using sol-gel method. The Cu^{2+}-doped TiO_2 film electrode was mainly in anatase phase. The as-prepared film coverage was quite uniform and the thickness of the films was about 2 μm. The EIS responses of the as-prepared film electrodes demonstrated that the photo-generated electron–hole pairs were efficiently separated by applying an external bias. The Cu^{2+}-doped TiO_2 film electrode had a high degradation rate for methylene blue and methyl orange with the help of an external bias under visible as well as UV light irradiation, due to the suppression of the recombination of photo-generated electron–hole pairs by the external electric field.

Acknowledgements

The authors acknowledge the supports of Shanghai Leading Academic Discipline Project (S30107), National Natural Science Foundation of China (Grant No. 51202138), Natural Science Foundation of Shanghai (Grant No. 12ZR1410500), Shanghai Environmental Research Program (2012–2007), Program of Shanghai Science and Technology Committee (11HX1188500), Shanghai Special Foundation for Cultivation of Youth Teacher from Universities, Research & Innovation Projects of Shanghai Education Commission (11YZ22), Science Foundation for Excellent Youth Scholars of Universities (Shanghai).

References

[1] X. Chen, S.S. Mao, Chemical Reviews 107 (2007) 2891–2959.
[2] K. Yasutaka, H. Yamashita, Journal of Materials Chemistry 21 (2011) 2407–2416.
[3] D. Nasuhoglu, V. Yargeau, D. Berk, Journal of Hazardous Materials 186 (2011) 67–75.
[4] M.H. Zhang, L.Y. Shi, S. Yuan, Y. Zhao, J.H. Fang, Journal of Colloid and Interface Science 330 (2009) 113–118.
[5] A. Panniello, M.L. Curri, D. Disod, A. Licciulli, V. Locaputo, A. Agostiano, R. Comparelli, G. Mascolo, Applied Catalysis B: Environmental 121/122 (2012) 190–197.
[6] R. Comparelli, E. Fanizza, M.L. Curri, P.D. Cozzoli, G. Mascolo, R. Passino, A. Agostiano, Applied Catalysis B: Environmental 55 (2005) 81–91.
[7] M.K. Aminian, N. Taghavinia, A. Irajizad, S.M. Mahdavi, Journal of Physical Chemistry C 111 (2007) 9794–9798.
[8] T. Kamegawa, Y. Shimizu, H. Yamashita, Advanced Materials 27 (2012) 3697–3700.
[9] A. Danion, J. Disdier, C. Guillard, N. Jaffrezic-Renault, Journal of Photochemistry and Photobiology A 190 (2007) 135–140.
[10] R. Kavitha, S. Meghani, V. Jayaram, Materials Science and Engineering B 139 (2007) 134–140.
[11] H. Zhang, H. Zhu, Applied Surface Science 258 (2012) 10034–10041.
[12] Y.J. Wang, J. Xu, W.Z. Zong, Y.F. Zhu, Journal of Solid State Chemistry 184 (2011) 1433–1438.
[13] P.S.M. Dunlop, A. Galdi, T.A. McMurray, J.W.J. Hamilton, L. Rizzo, J.A. Byrne, Journal of Advanced Oxidation Technologies 13 (2010) 99–106.
[14] N. Lu, X. Quan, J. Li, S. Chen, H. Yu, G. Chen, Journal of Physical Chemistry C 111 (2007) 11836–11842.
[15] Y. Su, S. Han, X. Zhang, X. Chen, L. Lei, Materials Chemistry and Physics 110 (2008) 239–246.
[16] H. Yang, C. Pan, Journal of Alloys and Compounds 501 (2010) 8–11.
[17] Y.J. Wang, J. Lin, R.L. Zong, J. He, Y.F. Zhu, Journal of Molecular Catalysis A: Chemical 349 (2011) 13–19.
[18] Y.F. Ma, M.Y. Xing, J.L. Zhang, B.Z. Tian, Microporous and Mesoporous Materials 156 (2012) 145–152.
[19] Y. Tu, S. Huang, J. Sang, X. Zou, Materials Research Bulletin 45 (2010) 224–229.
[20] H. Zhao, Y. Chen, X. Quan, X. Ruan, Chinese Science Bulletin 52 (2007) 1456–1461.
[21] L. Yu, S. Yuan, L.Y. Shi, Y. Zhao, J.H. Fang, Microporous and Mesoporous Materials 134 (2010) 108–114.
[22] K. Vinodgopal, S. Hotchandani, P.V. Kama, Journal of Physical Chemistry 97 (1993) 9040–9044.
[23] H.J. Choi, M. Kang, International Journal of Hydrogen Energy 32 (2007) 3841–3848.
[24] G. Li, N.M. Dimitrijevic, L. Chen, T. Rajh, K.A. Gray, Journal of Physical Chemistry C 112 (2008) 19040–19044.
[25] M. You, T.G. Kim, Y.M. Sung, Journal of Crystal Growth 10 (2010) 983–987.
[26] C. Rath, P. Mohanty, A.C. Pandey, N.C. Mishra, Journal of Physics D: Applied Physics 42 (2009) 205101–205107.
[27] R. Schaub, P. Thostrup, N. Lopez, et al., Physical Review Letters 87 (2001) 266104–266107.
[28] F. Fabregat-Santiago, E.M. Barea, J. Bisquert, G.K. Mor, K. Shankar, C.A. Grimes, Journal of the American Chemical Society 130 (2008) 11312–11316.
[29] O. Carp, C.L. Huisman, A. Reller, Prog, Solid State Chemistry 32 (2004) 33–177.
[30] L. Yu, Z.Y. Wang, L.Y. Shi, S. Yuan, Y. Zhao, J.H. Fang, W. Deng, Applied Catalysis B: Environmental 113–114 (2012) 318–325.
[31] Y.Z. Zhang, X.Y. Xiong, Y. Han, X.H. Zhang, F. Shen, S.H. Deng, H. Xiao, X.Y. Yang, G. Yang, H. Peng, Chemosphere 88 (2012) 145–154.
[32] H. Nishikiori, T. Sato, S. Kubota, N. Tanaka, Y. Shimizu, T. Fujii, Research on Chemical Intermediates 38 (2012) 595–613.
[33] M.D. Ward, A.J. Bard, Journal of Physical Chemistry 86 (1982) 3599–3605.
[34] U.B. Cappel, S.M. Feldt, J. Schoneboom, A. Hagfeldt, G. Boschloo, Journal of the American Chemical Society 132 (2010) 9096–9101.
[35] J. Li, L. Zheng, L. Li, Y. Xian, L. Jin, Journal of Hazardous Materials 139 (2007) 72–78.
[36] M.R. Hoffmann, S.T. Martin, W. Choi, D.W. Bahneman, Chemical Reviews 95 (1995) 69–96.
[37] C.A. Martínez-Huitle, E. Brillas, Applied Catalysis B: Environmental 87 (2009) 105–145.
[38] D. Jiang, H. Zhao, S. Zhang, R. John, Journal of Photochemistry and Photobiology A 177 (2006) 253–260.